TRANSMISSION OF MECHANICAL STRESSES WITHIN THE CYTOSKELETON OF ADHERENT CELLS: A THEORETICAL ANALYSIS BASED ON A MULTI-COMPONENT CELL MODEL

Philippe Tracqui[1] and Jacques Ohayon

Laboratoire TIMC-IMAG, Equipe DynaCell, - CNRS UMR 5525, Institut de l'Ingénierie et de l'Information de Santé, **I**n^3**S**, Faculté de médecine, 38706 La Tronche Cedex, France.

[1]Address for correspondence: Equipe Dynacell - Laboratoire TIMC-IMAG - CNRS UMR 5525, Institut de l'Ingénierie et de l'Information de Santé, **I**n^3**S**, Faculté de médecine, 38706 La Tronche cedex, France. Email: Philippe.Tracqui@imag.fr

ABSTRACT

How environmental mechanical forces affect cellular functions is a central problem in cell biology. Theoretical models of cellular biomechanics provide relevant tools for understanding how the contributions of deformable intracellular components and specific adhesion conditions at the cell interface are integrated for determining the overall balance of mechanical forces within the cell. We investigate here the spatial distributions of intracellular stresses when adherent cells are probed by magnetic twisting cytometry. The influence of the cell nucleus stiffness on the simulated nonlinear torque-bead rotation response is analyzed by considering a finite element multi-component cell model in which the cell and its nucleus are considered as different hyperelastic materials. We additionally take into account the mechanical properties of the basal cell cortex, which can be affected by the interaction of the basal cell membrane with the extracellular substrate. In agreement with data obtained on epithelial cells, the simulated behaviour of the cell model relates the hyperelastic response observed at the entire cell scale to the distribution of stresses and strains within the nucleus and the cytoskeleton, up to cell adhesion areas. These results, which indicate how mechanical forces are transmitted at distant points through the cytoskeleton, are compared to recent data imaging the highly localized distribution of intracellular stresses.

Keywords: Cell adhesion, Cytomechanical model, Twisting magnetocytometry, Finite Element Model, Hyperelasticity, Intracellular stress maps, Cell Monolayer homogenisation.

1. INTRODUCTION

In living tissues, cells are inevitably exposed to a variety of mechanical stresses and strains. Thus one of the fundamental questions in cell biology is how localized deformations in the extracellular matrix (ECM) induce and control cell and nucleus shapes (Pourati *et al.,* 1998). ECM-dependent shape control is critical for cell growth (Folkman and Greenspan, 1975), differentiation (Mooney *et al.,* 1992), and establishment of cell polarity and development of tissue pattern. Changes in cell shape

Acta Biotheoretica **52:** 323–341, 2004.

are commonly associated with alterations of nuclear structure (Ingber, 2000) which, in turn, appear to be required for changes in nuclear functions, including gene expression, nuclear transport or initiation of neoplastic transformation (Pienta *et al.,* 1991). ECM molecules, such as fibronectin, collagen or fibrin, produce cell shape changes via binding to cell surface integrin receptors which span the membrane and interconnect with actin microfilaments inside the cell (Janmey, 1998). Structural coupling between ECM, integrins and actin microfilaments suggests that the effects of ECM on cell shape are mediated via alterations in the cytoskeleton. In fact, great advances have been made in terms of identifying cytoskeletal components (e.g. talin, vinculin, α-actinin, paxillin) that interlink integrins with microfilaments. However, the mechanism by which local ligation of integrins results in cytoskeletal reorganization and global changes of cell shape remains unclear. Even less is known about how ECM promotes coordinated changes in cell and nuclear structure that are commonly observed in living cells.

It has been shown that when integrins were pulled by micromanipulating bound microbeads, cytoskeletal filaments reoriented, nuclei distorted, and nucleoli redistributed along the axis of the applied tension field (Maniotis *et al.,* 1997). Direct linkages between the cytoskeleton and nucleus mediate these effects. Molecular connections between integrins, cytoskeletal filaments, and nuclear scaffolds may therefore provide a discrete path for mechanical signal transfer through cells as well as a mechanism for producing integrated changes in cell and nuclear structure in response to changes in extracellular matrix adhesivity or mechanics (Hamill and Martignac, 2001).

More recently, Chen *et al.* (2001) reported the large increase of endothelin-1 gene expression in endothelial cells submitted to magnetic twisting stimulations. Moreover, twist-induced ET-1 gene expression is abolished when actin cytoskeleton is disrupted with Cytochalasin D or when cell prestress is modified using an inhibitor of the myosin ATPase which interferes with the actomyosin-based cystoskeleton contractility (Chen *et al.,* 2001). This experimental work exemplifies the interest of the magneto twisting cytometry (MTC) approach in the study of mechanotransduction pathways within the cell (Wang *et al.,* 1993; Wang and Ingber, 1994; Hubmayr *et al.,* 1996; Potard *et al.*, 1997). It also underlines that the knowledge of the extent to which strains propagate within the cell is crucial in this context and appears as a pre-requisite for understanding how gene expression is controlled by the transmission and magnitude of intracellular mechanical signals.

Indeed, if proteins and other chemical factors capable of modulating this global and bi-directional cell-signalling scheme have been identified, it is still not clear which magnitude and spatial distribution of intracellular strains and stresses permit or impair the transmission of such mechanical signals deeper in the cell. The role of intracellular components as mechanical buffers or enhancers is also largely unclear. Recently, the cell nucleus has received increased attention (Maniotis *et al.,* 1997; Guilak *et al.,* 2000; Caille *et al.,* 2002), but cell-substratum attachments have also been shown to modulate cell stiffness (Choquet *et al.,* 1997) and thus strains transmission.

In this context, theoretical models of the cell are of special interest for analyzing the modulation of the cell mechanical response when intracellular rheological properties and cell adhesion conditions are varied. A wide range of models has been proposed, from one-dimensional, rheological models based on springs and dashpots

associations (Wang and Ingber, 1994; Bausch *et al.,* 2001; Laurent *et al.,* 2003) to tensegrity structures (Stamenovic *et al.,* 1996; Ingber, 1997; Wendling *et al.,* 1999, 2000; Stamenovic and Coughlin, 2000; Cañadas *et al.,* 2002) or 3D continuum models (Caille *et al.,* 2002; Charras and Horton, 2002; Mijailovich *et al.,* 2002; Ohayon and Tracqui, 2004). This latter continuum approach appears as the most suitable to model the experimental context of the MTC experiments (Ohayon *et al.*, 2004). Indeed, the stress-strain relationship measured with MTC is fundamentally an average response resulting from the mechanical behaviour of a confluent (i.e. continuous) cell monolayer, which may thus be viewed as a unique continuum.

Our study presents a three-dimensional finite element model of the cell-bead linked structures, with appropriated contact conditions imposed at the cell-bead interface. The material parameters of the cellular model are taken from previous bead rotation-magnetic torque data obtained in living epithelial alveolar cells, cultured over coated rigid substrate and submitted to transient bead twisting (Laurent *et al.,* 2002; Ohayon *et al.*, 2004). In order to investigate the different mechanical contributions of various cell components, especially the nucleus, on the hyperelastic response observed when cells are probed by MTC (Laurent *et al.,* 2002), we analyze here the theoretical response of a simplified heterogeneous cell architecture composed of three intracellular elements, the nucleus, the basal cell cortex and the remaining cell cytoplasm, each of them being characterized by specific geometry and elastic properties. If geometrical parameters can be obtained rather easily, only limited information exists on the rheological properties of these cell components (Xu *et al.,* 2000). Maniotis *et al.* (1997) found that the nucleus is about nine times stiffer than the cytoplasm. Studies on isolated nuclei, using a micropipette aspiration technique, have shown that the elasticity of the nucleus, compared to that of the cytoplasm, is about ten times larger in neutrophil (Dong *et al.,* 1991), and about four times larger in chondrocytes (Guilak *et al.,* 2000). Caille *et al.* (2002) reported elastic moduli ranging from 1 kPa to 10 kPa in spread endothelial cells.

Based on this range of values, a finite element method is used in this paper to simulate the nonlinear increase of bead rotation in response to increasing magnetic torque. In order to obtain a constitutive law that well describes the nonlinear experimental response of the cells, we assumed that all materials are continuous, homogeneous, quasi-incompressible, isotropic and hyperelastic. For given bead rotations, the associated intracellular strain maps are simulated for different rheological parameters of the cell nucleus and the basal cell cortex. Different patterns of cell adhesion are also considered as a theoretical basis for discussing how the analysis of stress distributions in the cell-substrate boundary layer, i.e. at a very elementary subcellular scale, is integrated and related to the elastic response observed at the entire cell scale.

2. METHODS

Magnetic Twisting Cytometry (MTC)

The Magnetic Twisting Cytometry (MTC) method has originally been described by Wang *et al.* (1993) and tested extensively (Wang and Ingber, 1994). Briefly, ferromagnetic beads (3.5-5.5 μm diameter) coated with arginine-glycine-aspartic acid

(RGD) peptide bind to integrin transmembrane mechanoreceptors (Rahman *et al.,* 2002). Beads were then magnetized in the plane of the culture using a short uniform magnetic pulse. A magnetic torque is then created by a uniform vertical magnetic field resulting in a bead rotation, measured at equilibrium state, reflecting the cellular resistance induced by the cytoskeleton to the imposed deformation. Basically, this method provides the average bead rotation angle estimated over 10^5 beads bounded to about $5x10^4$ adherent cells (Laurent *et al.,* 2002).

Finite element analysis

Homogenization approach

In agreement with the experimental setup of Laurent *et al.* (2002) and assuming uniform distributions of cells and beads, we were able to define, for the studied cell monolayer culture, a representative cellular volume element (RCVE) of basal surface of size a x $2a$ where a is equal to 18 μm (Figure 1). Each cell was therefore represented by one RCVE, each RCVE including two beads and having a volume of a x $2a$ x h. By using the value of the mean cellular volume obtained by Schneider *et al*. (2000) in dog kidney epithelial cells (i.e., 2500 ± 300 μm^3), we were able to derive a mean cellular thickness value of $h = 4$ μm. Additionally, an ellipsoidal volume of revolution and a basal thin layer are included in the RCVE in order to model the cell nucleus and the basal cell cortex, respectively (Figure 2).

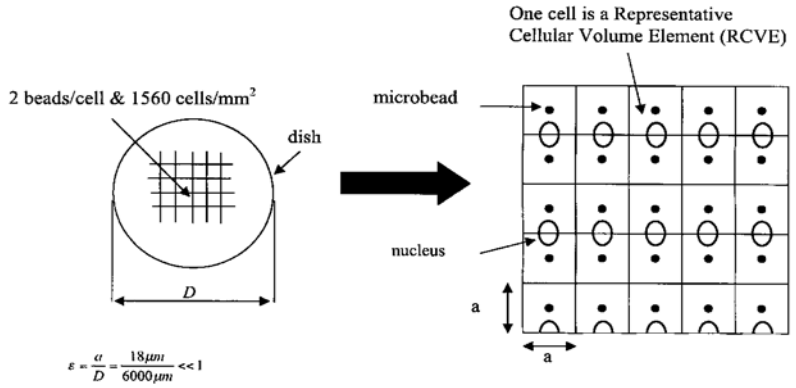

Figure 1. Description of the homogenization approach (left side): Schematic view of the cell culture where the cells are confluent with a density of 1560 cells/mm^2 and for an average bead density of two beads/cell (Laurent *et al*., 2002). Right side: Implementation of the homogenization concept. By definition, the RCVE (with size a x $2a$) scales the cellular medium and is thus able to reconstruct, by iterated duplications, the overall cell monolayer. This concept requires: (i) periodic boundary conditions; and (ii) a RCVE size which must be much smaller than the cell monolayer dimension, i.e. $a/D << 1$ (D: petri dish diameter).

By definition, the RCVE scales the cellular medium and is thus able to generate, by multiple duplications, the cell monolayer (Figure 1). Note also that the RCVE concept requires periodic boundary conditions, because the cell monolayer is reconstructed by

self-replication of the RCVE geometry, boundary conditions and material properties. Thus the RCVE concept imposes specific constraints, but which appear quite appropriate to describe MTC experiments performed over a large number of confluent cells.

Model geometry

Using the symmetrical plane passing across the centre of the two beads of the RCVE, we restricted our analysis to half the RCVE (Figure 2). Eight geometrical parameters were specifically needed to characterize the studied cellular domain (Figure 2): (i) the bead radius R, (ii) the embedding angle α, (iii) the cell thickness h, (iv) the basal cell cortex thickness e, (v) the size of the RCVE a, and (vi) the three semi-axes a_x, a_y, a_z of the ellipsoidal cell nucleus. Table 1 gives the values of R, α, h, e, a, a_x, a_y, a_z we will further use as reference values. They are estimated from both cell images and from the literature. Estimations of the bead immersion angle could be obtained by 3D-reconstruction techniques of the cell cytoskeleton (CSK) (Fodil *et al.,* 2003), but for simplicity we considered half-immersed beads (embedding angle of 90°).

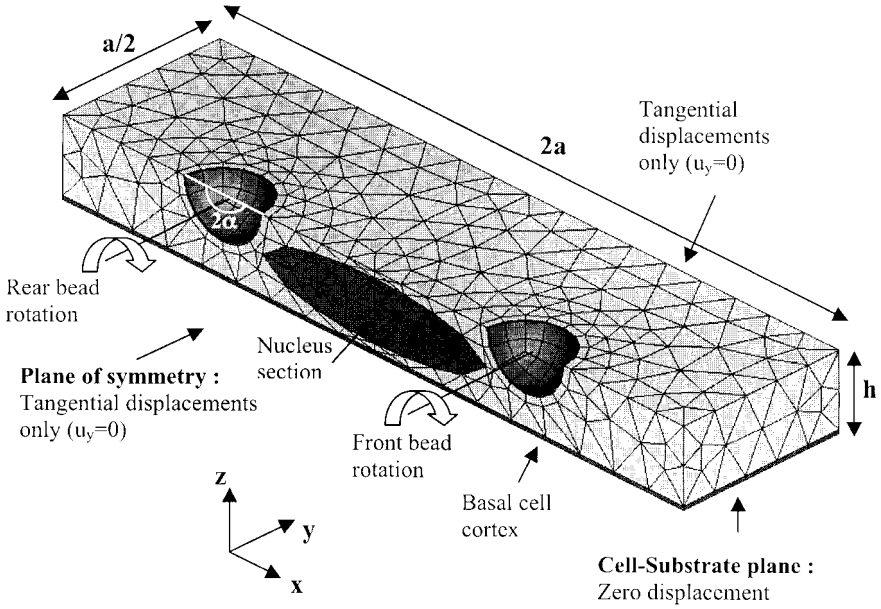

Figure 2. Finite element mesh of the half-representative cell volume element (RCVE) of size $a/2$ x $2a$ x h. The arrows indicate the orientation of the rotation applied at the beads centre. Only the bead prints are meshed. Free boundary conditions are applied to the RCVE surfaces except for displacement conditions explicitly indicated in the figure. Note that the RCVE includes the nucleus and the basal cell cortex. The angle α defines the bead embedding angle or half-angle of bead immersion (α = 90° here).

Table 1. Geometrical and rheological parameters defining the standard set of parameters used in the finite element simulations.

Standard set of geometrical and rheological parameters introduced in the model		
Geometry		
- Total cell thickness	$h = 4\ \mu$m	
- Basal cell cortex thickness	$e = 0.2\ \mu$m	
- Bead radius	$R = 2.25\ \mu$m	
- Bead embedding angle	$\alpha = 90°$ (i.e. half bead immersed)	
- Cell size (a x $2a$)	$a = 18\ \mu$m	
- Ellipsoidal nucleus		
(Equation: $x^2/a_x^2 + y^2/a_y^2 + z^2/a_z^2 = 1$)		
of semi-axes,	$a_x = 6.5\ \mu$m, $a_y = 5\ \mu$m, $a_z = 1.55\ \mu$m.	
Rheology **(quasi-incompressible medium)**		
- Cell	$a_{1c} = 3$ Pa,	$a_{2c} = 50$ Pa
- Basal cell cortex	$a_{1b} = 150$ Pa,	$a_{2b} = 0$ Pa
- Nucleus	$a_{1n} = 850$ Pa,	$a_{2n} = 0$ Pa

Boundary conditions

The boundary conditions were written on half of the RCVE (Figure 2). Displacement conditions were imposed on the cell boundaries:

(i) zero displacement, modeling full cell attachment to the substrate, was imposed on the basal cell membrane in contact with the rigid substrate,

(ii) free boundary conditions were assumed for the external apical cell surface, and

(iii) zero normal displacement condition was imposed on the cell section belonging to the plane of symmetry.

Moreover, in order to satisfy periodic boundary conditions on the RCVE: (i) free boundary conditions are considered for the two lateral cell surfaces and (ii) only tangential displacements are allowed on the border parallel to the plane of symmetry. All these boundary conditions are summarized in Figure 2.

Nonlinear elastic properties of the cell

In the light of the nonlinear stress-strain relationships given by MTC measurements, the cellular medium (i.e. the nucleus, the basal cortex, and the cytoskeleton), is assumed to be a hyperelastic, yet homogeneous, continuum (Ohayon *et al.*, 2004). Among the various strain-energy functions which can describe such a mechanical response, we retained the incompressible two parameter Yeoh like strain-energy function W (Holzapfel, 2001), already used to characterize tissues and living cells (Caille *et al.,* 2002). This strain-energy function is given by the following analytical expression (Holzapfel, 2001):

$$W = a_1(I_1 - 3) + a_2(I_1 - 3)^2, \quad (1)$$

where a_1 and a_2 are the two material constants, while I_1 is the first invariant of the right Cauchy-Green strain tensor C (I_1 = Trace(C)).

Finite element solutions

Computations of magnetic torque *vs* bead rotation and translation responses were performed using a finite element approach (Ansys 6.0 software, Ansys, Inc., Cannonsburg, Pennsylvania, USA). Simulations were performed in static conditions. The cell components were meshed with hyperelastic elements, considering typically ~2000 elements and ~4000 nodes.

Since the mesh (type and number of elements) can possibly affect the numerical results, a control of the numerical error is performed using as a test case the computation of the torque resulting from the rotation of a rigid spherical bead embedded in an infinite medium. For an imposed bead rotation, chosen in order to satisfy the small strains conditions, we checked that the computed torque value agreed within 0.6% with the theoretical value derived from the analytical torque expression (Phan-Thien, 1993).

3. RESULTS

While the geometrical features of the homogenised cell model (Table 1) can be mainly derived from the homogenization approach (see previous section), we need an additional hypothesis for estimating the rheological constants characterizing the elastic properties of the cell cytoskeleton (CSK), nucleus and basal cortex. Indeed, the choice of the retained strain energy function (Equation 1) requires the identification of a couple of parameters a_1, a_2 for each cell component, while MTC experiments only provide a global response which integrates the contribution of all these components. We therefore adopt the following approach: preliminary estimation of the CSK rheological constants (a_{1c}, a_{2c}) is obtained by considering the cell as a unique homogeneous medium and by adjusting the simulated cell response to the bead rotation-magnetic torque data obtained by MTC in living epithelial alveolar cells (Tracqui *et al.,* 2003). A satisfactory fit to the experimental data is obtained for the values of a_{1c} = 3 Pa and a_{2c} = 50 Pa. Regarding the cell nucleus rheology, we follow the results of Caille *et al.* (2002) who considered a strain energy function with a zero value of the rheological constant a_2. In this case, the expression of the initial Young's modulus is $6a_1$ (see Appendix 1). Thus, from the range of Young's modulus values reported in (Caille *et al.,* 2002) for the nucleus of spreading cells, i.e. 1 kPa to 10 kPa, we considered the average value a_{1n} = 850 Pa as the standard value for the nucleus rheological constant in our simulations. In a similar way, we assumed that the basal cell cortex rheology can be describe with only one rheological constant a_{1b}. A precise estimation of this constant is rather difficult since the rheology of actin polymers highly depends on the experimental conditions. In the simulations we consider a standard value a_{1b} = 150 Pa, which is in agreement with the values reported in the literature and ranging roughly from 1 kPa to 10 kPa. Table 1 compiles all the model parameters values defining the standard set (Std set) of parameters.

Influence of the nucleus stiffness

In order to analyse the effect of the elastic properties of the nucleus on the mechanical response, two simulations were performed (Figure 3) for the same rheology of the basal cell cortex. In the first one, the nucleus is much stiffer than the CSK (heterogeneous cell, Std parameter set), while in the second case (homogeneous

cell), the elastic properties of the cell nucleus and cell CSK are assumed to be the same. In both cases, the nonlinear aspect of the mechanical torque-bead rotation response appears clearly. As expected, the homogeneous cell is more compliant than the heterogeneous cell: for the same applied torque T, larger beads rotations are obtained compared to the heterogeneous cell case (Figure 3). Nevertheless, these two torque-bead rotation response curves remain rather close, even for large torque (i.e. normalized Torque/Bead volume values above 80 Pa) corresponding to the experimental values obtained in the MTC experiments (Laurent *et al.,* 2002). However, such qualitative and quantitative similarities in the integrated or global response correspond to very different mechanical contexts at the sub-cellular scale. Indeed, a more precise analysis of the spatial distributions of strains and stresses in the neighbourhood of the cell nucleus and basal cell cortex reveals significant differences.

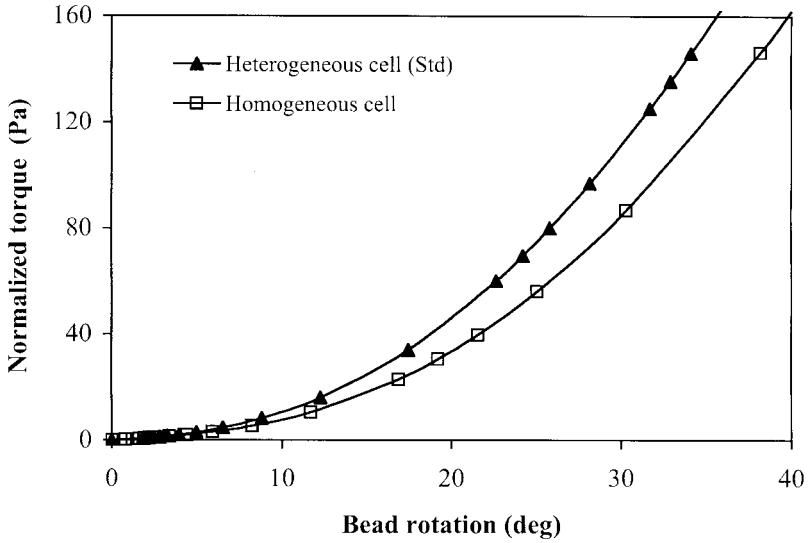

Figure 3. Influence of the nucleus stiffness on the mechanical torque-bead rotation response. The Heterogeneous cell curve is the control simulation obtained with the Std set of parameters defined in Table 1. The Homogeneous cell curve is obtained when considering that the cell nucleus and CSK have the same elastic properties. Normalized torque values are obtained by dividing the applied torque T by the bead volume V_b.

Figure 4 gives the deformed cell shape and 3D maps of spatial effective strain distribution within the heterogeneous cell when a rotation angle θ of 25° is applied to both beads. Maximal strain value of ~55% is observed for the CSK in the front of the rear bead. The amplitudes of the maximum effective strains are similar (~4%) in the nucleus and the basal cortex, but much smaller than in the CSK. Small but significant effective strains also appear under the stiff nucleus.

For the same imposed bead rotation of 25°, Figure 5 gives the corresponding deformed cell and nucleus shapes as well as the spatial distribution of the intracellular effective strains within the homogeneous cell. Compared to the previous case (Figure 4), the maximal strain of the CSK is lower (~37%) and now appears at the rear of the front bead. Conversely, the amplitude of the maximal effective strain in the

nucleus is now six times higher (~25%), while the maximal effective strain still remains quite small in the basal cortex (~4%). Interestingly, the basal cortex area below the soft nucleus is almost unstrained, indicating that compliant nucleus seems to prevent the strains propagation up to the cell-substrate interface. One can also notice that, even if the CSK and the nucleus have the same rheology, the spatial strains distribution in the neighbourhood of the front and rear beads respectively is not fully symmetrical. This underlines the existence of a weak interaction between the mechanical effects induced by the two beads. Such interactions, which could have potential implications in the data acquisition protocol, are more precisely analyzed in the next paragraph.

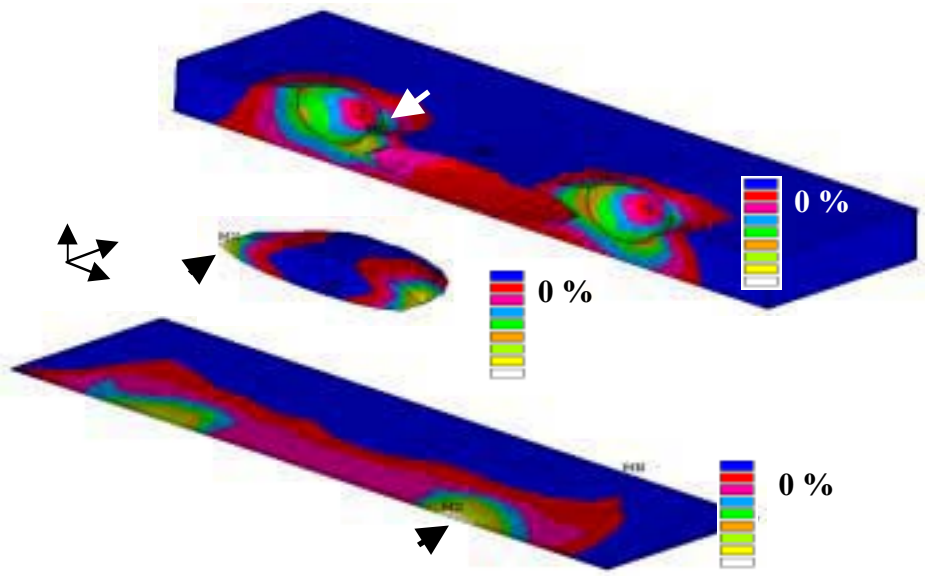

Figure 4. Deformed cell and nucleus shapes and associated 3D strain maps. The spatial distributions of the effective strain of the CSK (top view), nucleus (middle view) and basal cortex (bottom view) are given. The effective Lagrangian strain is given by $e_{eff} = \sqrt{2e_{ij}\, e_{ij}\,/3}$ (where e_{ij} are the components of the deviatoric strain tensor). These numerical results are obtained with the Std set of parameters and when a rotation of 25° is imposed on the two beads. A mean bead translation Δ_x in the Ox direction is associated with the bead rotation, with $\Delta_x = 0.45\ \mu$m. The resulting normalized mean torque is 75 Pa. The beads have been removed in order to visualize more clearly the spatial strain distributions around the cell-bead contact areas. Arrows indicate the maximum effective strain locations within each sub-cellular component.

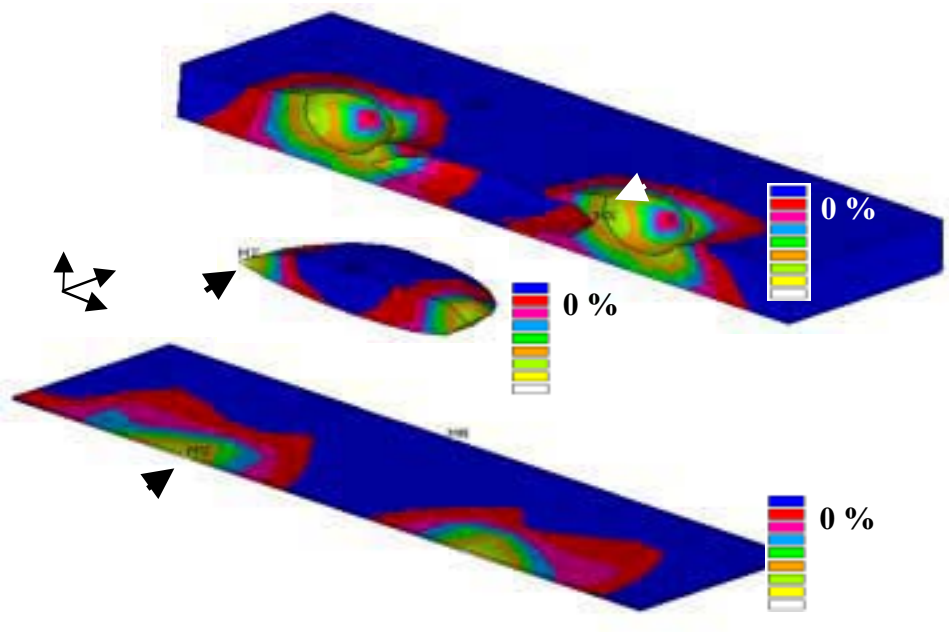

Figure 5. Legend as in Figure 4, except that the elastic properties of the nucleus are now those of the CSK. The 25° imposed rotation of the two beads induces a mean bead translation Δ_x of 0.54 μm. The resulting normalized mean torque is 56 Pa. Arrows indicate the maximum effective strain locations in each cell constituent.

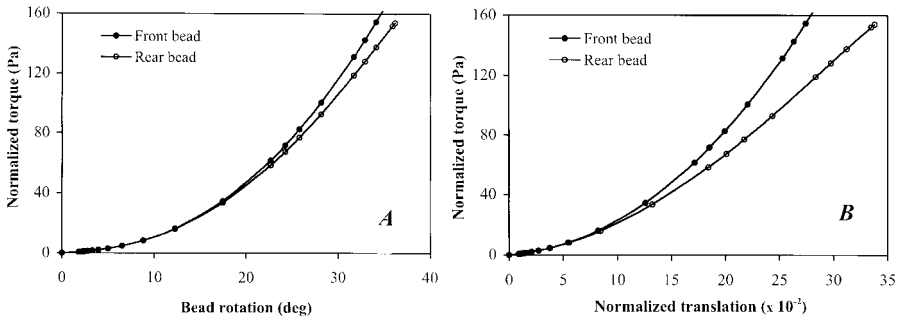

Figure 6. Mechanical response of the front and rear beads simulated with the Std set parameters. A) Nonlinear torque-bead rotation response curves. B) Nonlinear mechanical torque-bead translation response curves. The bead translation Δ_x is normalized by the bead radius *R*.

Differences between front and rear beads mechanical responses

In the Std case, i.e. when the nucleus is stiffer than the CSK, the front bead and the rear bead rotate to almost the same value when increasing torque values are applied (Figure 6A). One could thus expect the front and rear beads to have the same kinematic behaviour, but surprisingly, the translation of the rear bead is much larger than the one of the front bead (Figure 6B). In other words, the rear bead seems less affected by the stiff nucleus than the front bead. This phenomenon can be explained by considering the counter clockwise rotation of the nucleus which occurs in pace with the clockwise rotation of the beads: the rotation of the front bead tends to lift the front of the nucleus while on the contrary the rotation of the rear bead tends to lower the rear part of the nucleus. The rotation of the nucleus that results from this kinematic combination favours the translation of the rear bead.

Apparent cell stiffness and nonlinear elastic response

The different patterns of the intracellular strain maps discussed in the above section are controlled by the nonlinear elastic behaviour of adherent cells. This nonlinearity, mainly due to the nonlinear elastic properties of the cell constituents and not to geometrical nonlinearities, corresponds to an increasing resistance to the applied torque when this mechanical loading is applied directly to cell surface receptors by magnetically twisted surface-bound microbeads, as revealed by MTC data (Laurent *et al.,* 2002). This increase in cell stiffness with increasing applied stress or strain is known as the strain-hardening effect (Stamenovic *et al.,* 2000). Quantitatively, this resistance to mechanical load is usually measured by the so-called apparent stiffness E_{app}, which is defined as the ratio of the normalized applied torque T/V_b (T applied torque, V_b bead volume) over the associated bead rotation θ (Figure 7A). Let us remark that for the Std set of parameters, the nonlinearity of the cell medium affects the mechanical response even for a bead rotation angle as small as 10° (Figure 7A).

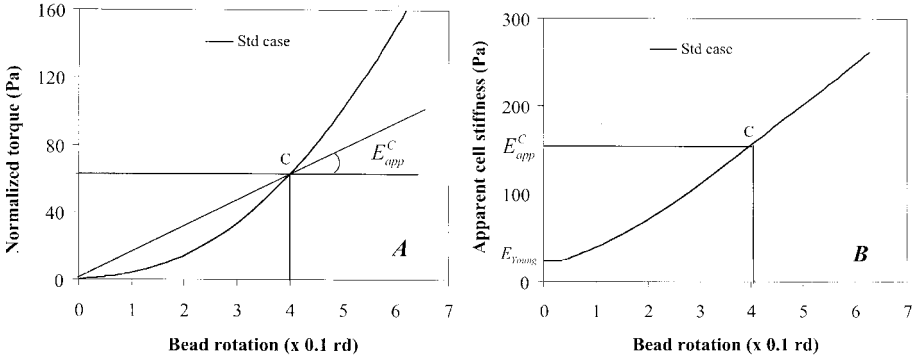

Figure 7. Simulated nonlinear elastic response of the adherent epithelial cells obtained with the Std set of parameters. A) Normalized torque-bead rotation response. The apparent cell stiffness E^C_{app} at a point C of the response curve is defined as the slope of the straight line 0C. The torque T is normalized by the bead volume V_b. B) Associated variation of the apparent cell stiffness E^C_{app} for increasing bead rotation derived from Figure 6A.

In this simulation, a linear domain, corresponding to an almost constant value of the apparent cell stiffness, can only be defined for bead rotation angles lower than 4° (Figure 7B).

Influence of the nucleus and basal cortex stiffnesses on strain amplitudes

Figure 8 shows that above 1 kPa, the nucleus Young's modulus has almost no effect on the maximum effective strains. However, below 1 kPa, the nucleus response becomes very sensitive to the bead rotation: the amplitudes of the maximal strain observed within the nucleus increases dramatically and reaches almost the value obtained within the CSK.

It is also below the 1 kPa value that changes of the basal cortex elasticity can significantly modify the maximal effective strains observed at this interface between the cell and its underlying substrate (Figure 9). Figure 10 illustrates the sensitivity of this mechanical response with regard to the basal cell cortex elasticity by comparing the curve obtained in the standard case (Young's modulus of 900 Pa) with the one obtained with a softer cortex (Young's modulus of 12 Pa). Additional computations show that the mechanical torque-rotation response is affected when the Young's modulus of the basal cortex is lower than 30 Pa. Interestingly, the maximal effective strains within the CSK and the nucleus are not affected by such changes of the basal cortex Young's modulus (Figure 9). Thus, the softening of the basal cortex appears as a means of concentrating the strain at the basal cell surface, which could have major implications for modulating cell-extracellular matrix or cell-cell interactions.

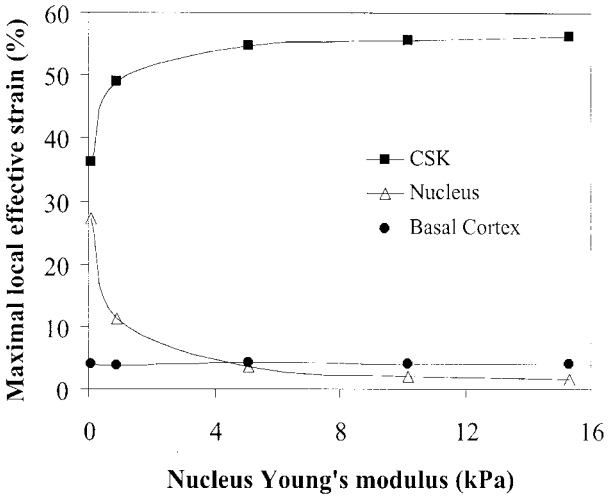

Figure 8. Influence of the nucleus stiffness on the amplitude of the maximal local effective strain in the different cell components. In all the simulations, the locations of the maximal effective strains are those indicated on Figure 4. These numerical results are obtained when a rotation of 25° is imposed on the two beads. All computations have been performed with the Std set of parameters except for the parameter under study, i.e. the nucleus Young's modulus.

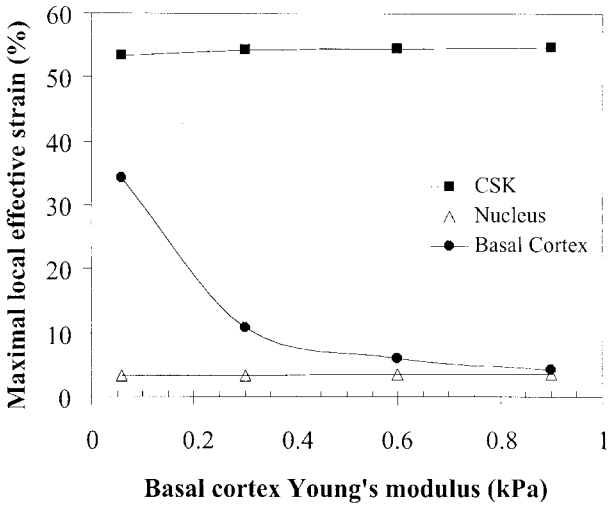

Figure 9. Influence of the basal cortex stiffness on the amplitude of the maximal local effective strain in the different cell components. In all the simulations, the locations of the maximal effective strains are those indicated on Figure 4. These numerical results are obtained when a rotation of 25° is imposed on the two beads. All computations have been performed with the Std set of parameters except for the parameter under study, i.e. the basal cortex Young's modulus.

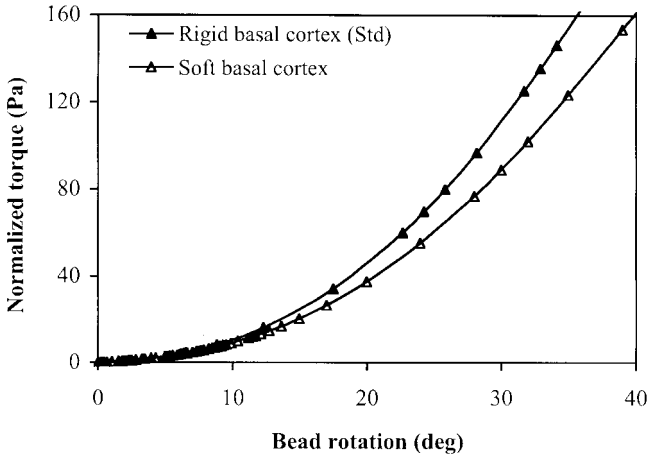

Figure 10. Influence of basal cortex stiffness on the hyperelastic torque-bead rotation response. The "Rigid basal cortex" curve is the control simulation obtained with the Std set of parameters (Table 1) with basal cortex Young's modulus $6a_{1b} = 900$ Pa. The "Soft basal cortex" curve is obtained with the same parameters, except for the basal cortex Young's modulus now equals to 12 Pa.

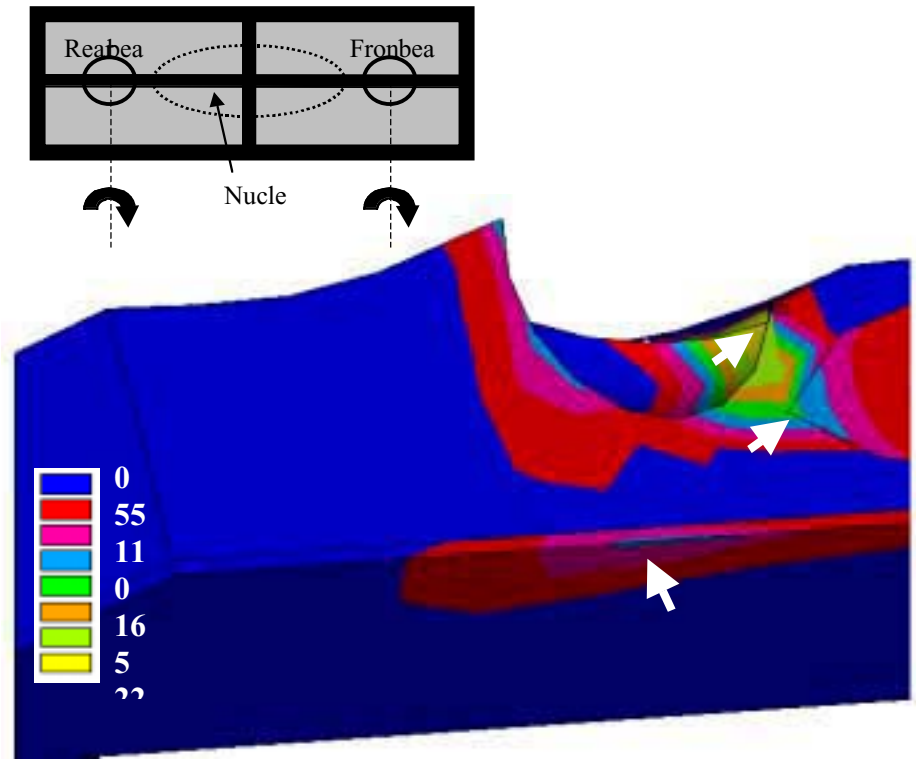

Figure 11. Influence of the cell adhesion pattern on the cell mechanical response. Upper insert: Schematic view of the RCVE and of the cell adhesion pattern considered in the simulation. Shaded areas correspond to a lack of cell adhesion and thick solid lines are the cell-substrate adhesion regions. The arrows indicate the orientation of the rotation applied at the beads centre. Bottom: Enlargement of the 3D stress map showing the heterogeneous spatial distribution of the Von-Mises stress fields σ_{eff} in the neighbourhood of the rear bead. These numerical results are obtained when a rotation of 25° is imposed on the two beads, inducing then a mean bead translation Δ_x of 0.45 μm. The resulting normalized mean torque is 74.5 Pa. The rear bead has been removed in order to more clearly visualize the spatial stress distributions around the cell-bead contact area. This computation has been performed with the Std set of parameters except for the basal cortex Young's modulus which is equal to 10.2 kPa. The Von-Mises stress (or effective stress) is given by $\sigma_{eff} = \sqrt{3 S_{ij} S_{ij} / 2}$ (where S_{ij} are the components of the deviatoric stress tensor). Arrows indicate the maximal Von-Mises stress locations within each cell component.

Influence of cell-substrate adhesion surface on the intracellular stress distribution patterns

Mechanical stresses exerted by adherent cells are transmitted to the underlying extracellular matrix through localized focal adhesion structures. In order to analyse how such localized structures of the cell basal surface would respond to stress applied

at the apical surface, we considered a simplified heterogeneous pattern of cell adhesion (Figure 11, insert). Cell adhesion onto the substrate occurs mainly at the cell periphery, but also transversally, as it could be suggested by 3D-reconstruction of actin cytoskeleton (Fodil *et al.,* 2003). We then simulated the intracellular stress distribution obtained when a rotation of 25° is imposed on both magnetic beads (Figure 11), the model parameters being fixed to their Std set values. For this imposed rotation, the associated mean bead translation is 0.45 μm. An enlargement of the stress map in the neighbourhood of the rear bead is given in Figure 11. As in Figure 4, maximal mechanical effects are obtained in front of the bead and at the rear part of the nucleus, with stress values in a range of 400 - 500 Pa. Quite interestingly, the stress values drastically decrease below the bead and then exhibit a sharp increase (~300 Pa) within the facing basal cortex area. Thus, despite the continuous architecture of the intracellular cell medium, the stress propagation within the cell appears as discontinuous.

4. DISCUSSION

The mechanical properties of living cells have been repeatedly reported as key controlling factors for both cell dynamics and intracellular transduction pathways. Even if the experimental context is quite different from the *in vivo* situations experienced by cells embedded in a three-dimensional extracellular matrix, *in vitro* micromanipulations of adherent cells are of great interest for analysing the balance of mechanical forces which result from the tension generated by the cytoskeleton and the mechanical resistance created by cell attachments to the underlying substrate. Based on the finite element formulation of a hyperelastic model of the cell deformation, this paper provides an original analysis of the intracellular stress and strain propagation to focal adhesion regions in response to a localized load applied at the apical cell surface. This analysis has been undertaken with reference to the experimental framework defined by magnetic twisting cytometry and has taken benefit from the homogenisation approach which can be successfully used to derive an homogenised cell model from the geometry of the probed confluent cell monolayer. Our homogenised cell model mimics a simplified cell architecture composed of three materials with different elastic properties, namely the cytoskeleton, the nucleus and the basal cell cortex. The influence of these components of the cell architecture on the cell response to simulated bead rotation has been investigated for different ratio of the elasticity moduli of each sub-structure. Taken together, our results highlight different strategies which could be used by the cell to overcome and adapt stress. The strain hardening properties of the CSK tends to enhance the distance over which the intracellular deformations propagate. This phenomenon appears of great importance for evaluating the efficiency with which mechanical signals are transmitted to the cell nucleus and to focal adhesion sites. The intracellular 3D maps established from our simulations quantify precisely the intracellular strain distribution from the apical to the basal cell surface. By considering simplified cell adhesion patterns, we furthermore illustrated how such intracellular propagation of the strain hardening can be monitored by topological changes of cell adhesion onto the underlying rigid substrate. In our study, the strain heterogeneity is due to a direct mechanical response, but it could also

be coupled to a biochemical remodelling response of the CSK or of basal cortex layer, especially when cell adhesion is realized on deformable extracellular substrates.

Our finite element modelling of cell mechanics also provides a qualitative and quantitative basis for improving the validity of cell cytomechanical models through comparison between continuum approaches and discrete models, like tensegrity strucures, for which strain hardening properties have been reported (Wendling *et al.,* 1999; Chen *et al.,* 2001). Our simulations are consistent with recent work of Hu *et al.* (2003) who visualized the discontinuous aspect of the strains distribution below the rotating bead in MTC experiments. These authors reported that the observed stress transfer patterns are strongly dependent on focal adhesions and postulated a cellular transmission of forces by a tensed cable network insuring preferential connections between the load site and the maximal stress. We reported here a similar discontinuity of the intracellular stress maps when considering a continuous medium, but for given ratios of the CSK and basal cortex elasticity.

Our analysis of the influence of cell adhesion patterns could furthermore provide some theoretical guidelines and predictions for analysing the large body of experimental data indicating that focal adhesion complexes are regulated in structure and size in response to mechanical loading (Wozniak *et al.,* 2000; Balaban *et al.,* 2001; Schwarz *et al.,* 2002).

ACKNOWLEDGEMENTS

This work is supported by a grant “Bio-informatique” from the French Centre National de la Recherche Scientifique.

NOMENCLATURE

a:	Side length of the representative cellular volume element
a_1:	First rheological constant of the Yeoh strain energy function
a_2:	Second rheological constant of the Yeoh strain energy function
a_x, a_y, a_z:	Semi-axes of the ellipsoidal nucleus in the x, y and z directions, respectively
e:	Thickness of the basal cortex layer
e_{eff}:	Local effective strain field
e_{ij}:	Components of the deviatoric strain field
h:	Cell thickness
$\vec{u}$:	Displacement vector of components u_i
(x,y,z):	Coordinates associated with the cartesian base
C:	Right Cauchy-Green strain tensor
E:	Lagrangian strain tensor of components E_{ij}
E_{app}:	Apparent cell stiffness
E_{cell}:	Young’s modulus obtained from an uniaxial extension and compression test
I_1:	First invariant of the right Cauchy-Green strain tensor C
R:	Bead radius
S_{ij}:	Components of the deviatoric stress tensor
T:	External torque applied

V_b: Bead volume
W: Strain energy function for hyperelastic material
α: Half-angle of bead immersion or embedding angle
θ: Bead rotation
λ: Extension ratio
σ_{eff}: Von-Mises stress or local effective stress
Δ_x: Bead translation in the ox direction

REFERENCES

Balaban, N.Q., U.S. Schwarz, D. Riveline, P. Goichberg, G. Tzur, I. Sabanay, D. Mahalu, S. Safran, A. Bershadsky, L. Addadi *et al.* (2001). Force and focal adhesion assembly: a close relationship studied using elastic micropatterned substrates. Nature in Cell Biology 3: 466-72.

Bausch, A.R., U. Hellerer, M. Essler, M. Aepfelbacher and E. Sackmann (2001). Rapid stiffening of integrin receptor-actin linkages in endothelial cells stimulated with thrombin: a magnetic bead microrheology study. Biophysical Journal 80: 2649-57.

Caille, N., O. Thoumine, Y. Tardy and J.J. Meister (2002). Contribution of the nucleus to the mechanical properties of endothelial cells. Journal of Biomechanics 35: 177-87.

Canadas, P., V.M. Laurent, C. Oddou, D. Isabey and S. Wendling (2002). A cellular tensegrity model to analyse the structural viscoelasticity of the cytoskeleton. Journal of Theoretical Biology 218: 155-73.

Charras, G.T. and M.A. Horton (2002). Determination of cellular strains by combined atomic force microscopy and finite element modeling. Biophysical Journal 83: 858-79.

Chen, J., B. Fabry, E.L. Schiffrin and N. Wang (2001). Twisting integrin receptors increases endothelin-1 gene expression in endothelial cells. American Journal of Physiology-Cell Physiology 280: C1475-84.

Choquet, D., D.P. Felsenfeld and M.P. Sheetz (1997). Extracellular matrix rigidity causes strengthening of integrin-cytoskeleton linkages. Cell 88: 39-48.

Dong, C., R. Skalak and K.L. Sung (1991). Cytoplasmic rheology of passive neutrophils, Biorheology 28: 557-67.

Fodil, R., V. Laurent, E. Planus and D. Isabey (2003). Characterization of cytoskeleton mechanical properties and 3D-actin structure in twisted adherent epithelial cells. Biorheology 40: 241-5.

Folkman, J. and H.P. Greenspan (1975). Influence of geometry on control of cell growth. Biochemica and Biophysica Acta 417: 211-36.

Guilak, F., J.R. Tedrow and R. Burgkart (2000). Viscoelastic properties of the cell nucleus. Biochemical and Biophysical Research Communications 269: 781-6.

Hamill, O.P. and B. Martinac (2001). Molecular basis of mechanotransduction in living cells. Physiological Review 81: 685-740.

Holzapfel, G.A (2001). Nonlinear Solid Mechanics: Wiley & Sons, Chichester.

Hu, S., J. Chen, B. Fabry, Y. Numaguchi, A. Gouldstone, D.E. Ingber, J.J. Fredberg , J.P. Butler and N. Wang (2003). Intracellular stress tomography reveals stress focusing and structural anisotropy in cytoskeleton of living cells, American Journal of Physiology-Cell Physiology 285: C1082-1090.

Hubmayr, R.D., S.A. Shore, J.J. Fredberg, E. Planus, R.A. Panettieri Jr., W. Moller, J. Heyder and N. Wang (1996). Pharmacological activation changes stiffness of cultured human airway smooth muscle cells. American Journal of Physiology 271: C1660-8.

Ingber, D.E (1997). Tensegrity: the architectural basis of cellular mechanotransduction. Annual Review of Physiology 59: 575-99.

Ingber, D.E (2000). Opposing views on tensegrity as a structural framework for understanding cell mechanics. Journal of Applied Physiology 89: 1663-70.

Janmey, P.A (1998). The cytoskeleton and cell signaling: component localization and mechanical coupling. Physiological Reviews 78: 763-81.

Laurent, V.M., E. Planus, R. Fodil and D. Isabey (2003). Mechanical assessment by magnetocytometry of the cytosolic and cortical cytoskeletal compartments in adherent epithelial cells. Biorheology 40: 235-40.

Laurent, V.M., S. Henon, E. Planus, R. Fodil, M. Balland, D. Isabey and F. Gallet (2002). Assessment of mechanical properties of adherent living cells by bead micromanipulation: comparison of magnetic twisting cytometry vs optical tweezers. Journal of Biomechanical Engineering 124: 408-21.

Maniotis, A.J., C.S. Chen and D.E. Ingber (1997). Demonstration of mechanical connections between integrins, cytoskeletal filaments, and nucleoplasm that stabilize nuclear structure. Proceedings of the National Academy of Sciences USA 94: 849-54.

Mijailovich, S.M., M. Kojic, M. Zivkovic, B. Fabry and J.J. Fredberg (2002). A finite element model of cell deformation during magnetic bead twisting. Journal of Applied Physiology 93: 1429-36.

Mooney, D., L. Hansen, J. Vacanti, R. Langer, S. Farmer and D. Ingber (1992). Switching from differentiation to growth in hepatocytes: control by extracellular matrix. Journal of Cell Physiology 151: 497-505.

Ohayon, J. and P. Tracqui (2004). Computation of Adherent Cell Elasticity for Critical Cell-Bead Geometry in Magnetic Twisting Experiments. Annals of Biomedical Engineering: In press.

Ohayon, J., P. Tracqui, R. Fodil, S. Féréol, V. Laurent, E. Planus and D. Isabey (2004). Analysis of nonlinear responses of adherent epithelial cells probed by magnetic bead twisting: a finite element model based on an homogenization approach. Journal of Biomechanical Engineering: In press.

Phan-Thien, N (1993). Rigid spherical inclusion: the multiple expansion. Journal of Elasticity 32: 243-52.

Pienta, K.J., B.C. Murphy, R.H. Getzenberg and D.S. Coffey (1991). The effect of extracellular matrix interactions on morphologic transformation in vitro. Biochemical Biophysical Research Communications 179: 333-9.

Potard, U.S., J.P. Butler and N. Wang (1997). Cytoskeletal mechanics in confluent epithelial cells probed through integrins and E-cadherins. American Journal of Physiology 272: C1654-63.

Pourati, J., A. Maniotis, D. Spiegel, J.L. Schaffer, J.P. Butler, J.J. Fredberg, D.E. Ingber, D. Stamenovic and N. Wang (1998). Is cytoskeletal tension a major determinant of cell deformability in adherent endothelial cells? American Journal of Physiology 274: C1283-9

Rahman, A., Y. Tseng and D. Wirtz (2002). Micromechanical coupling between cell surface receptors and RGD peptides. Biochemical and Biophysical Research Communications 296: 771-8.

Schneider, S.W., P. Pagel, C. Rotsch, T. Danker, H. Oberleithner, M. Radmacher and A. Schwab (2000). Volume dynamics in migrating epithelial cells measured with atomic force microscopy. Pflugers Archives 439: 297-303.

Schwarz, U.S., N.Q. Balaban, D. Riveline, A. Bershadsky, B. Geiger and S.A. Safran (2002). Calculation of forces at focal adhesions from elastic substrate data: the effect of localized force and the need for regularization. Biophysical Journal 83: 1380-94.

Stamenovic, D. and M.F. Coughlin (2000). A quantitative model of cellular elasticity based on tensegrity. Journal of Biomechanical Engineering 122: 39-43.

Stamenovic, D., D.E. Ingber, N. Wang and J.J. Fredberg (1996). A Microstructural Approach to Cytoskeletal Mechanics based on Tensegrity. Journal of Theoretical Biology 181: 125-136.

Tracqui, P., J. Ohayon, R. Fodil, E. Planus, V.M. Laurent and D. Isabey (2003). Strain hardening response of adherent epithelial cells micromanipulated by magnetic bead twisting. 28ème Congrès de la Société de Biomécanique, Poitiers.

Wang, N. and D.E. Ingber (1994). Control of cytoskeletal mechanics by extracellular matrix, cell shape, and mechanical tension. Biophysical Journal 66: 2181-9.

Wang, N., J.P. Butler and D.E. Ingber (1993). Mechanotransduction across the cell surface and through the cytoskeleton. Science 260: 1124-7.

Wendling, S., C. Oddou and D. Isabey D (1999). Stiffening response of a cellular tensegrity model. Journal of Theoretical Biology 196: 309-25.

Wendling, S., E. Planus, V.M. Laurent, L. Barbe, A. Mary, C. Oddou and D. Isabey (2000). Role of cellular tone and microenvironment on cytoskeleton stiffness predicted by tensegrity model. European Physical Journal of Applied Physics 9: 51-62.

Wozniak, M., A. Fausto, C.P. Carron, D.M. Meyer and K.A. Hruska (2000). Mechanically strained cells of the osteoblast lineage organize their extracellular matrix through unique sites of alphavbeta3-integrin expression. Journal of Bone and Mineral Research 15: 1731-45.

Xu, J., Y. Tseng and D. Wirtz (2000). Strain hardening of actin filament networks. Regulation by the dynamic cross-linking protein alpha-actinin. Journal of Biological Chemistry 275: 35886-92.

APPENDIX 1

Derivation of a Young's modulus in uniaxial test

One can infer the strain dependent Young's modulus E_{cell} values from the two Mooney-Rivlin material parameters a_1 and a_2 by considering the medium response to uniaxial tension and compression. The derived analytical expression of E_{cell} is then given by the equation:

$$E_{cell}(a_1, a_2, \lambda) = 2a_1(2 + \frac{1}{\lambda^3}) + 4a_2(4\lambda^2 - 6 + \frac{1}{\lambda} - \frac{3}{\lambda^3} + \frac{4}{\lambda^4}) \qquad \text{(A1)}$$

where λ is the extension ratio in direction of the uniaxail stress, which is related to the lagrangian strain component E_{11} in the same direction by the equation $\lambda = \sqrt{2E_{11} + 1}$. Note that for small extension, we have $\lambda \sim 1$ and therefore $E_{cell} \sim 6\, a_1$. The strain hardening behavior is more pronounced during compression than during tension. Interestingly, the variation of E_{cell} with E_{11} is linear for large positive strains ($\lambda >> 1$), with slope dE_{cell}/dE_{11} equals to $32\, a_2$.